A vertically integrated model with vertical dynamics for CO2 storage

AGU PUBLICATIONS

Water Resources Research

RESEARCH ARTICLE
10.1002/2013WR015215

Key Points:
- A vertically integrated model with vertical dynamics is developed
- It extends the applicability of vertically integrated models for CO_2 storage
- It maintains most computational advantages of vertical equilibrium models

Correspondence to:
B. Guo,
boguo@princeton.edu

Citation:
Guo, B., K. W. Bandilla, F. Doster, E. Keilegavlen, and M. A. Celia (2014), A vertically integrated model with vertical dynamics for CO_2 storage, *Water Resour. Res.*, *50*, 6269–6284, doi:10.1002/2013WR015215.

Received 23 DEC 2013
Accepted 4 JUL 2014
Accepted article online 10 JUL 2014
Published online 4 AUG 2014

A vertically integrated model with vertical dynamics for CO_2 storage

Bo Guo[1], Karl W. Bandilla[1], Florian Doster[1,2], Eirik Keilegavlen[1,2], and Michael A. Celia[1]

[1]Department of Civil and Environmental Engineering, Princeton University, Princeton, New Jersey, USA, [2]Department of Mathematics, University of Bergen, Bergen, Norway

Abstract Conventional vertically integrated models for CO_2 storage usually adopt a vertical equilibrium (VE) assumption, which states that due to strong buoyancy, CO_2 and brine segregate quickly, so that the fluids can be assumed to have essentially hydrostatic pressure distributions in the vertical direction. However, the VE assumption is inappropriate when the time scale of fluid segregation is not small relative to the simulation time. By casting the vertically integrated equations into a multiscale framework, a new vertically integrated model can be developed that relaxes the VE assumption, thereby allowing vertical dynamics to be modeled explicitly. The model maintains much of the computational efficiency of vertical integration while allowing a much wider range of problems to be modeled. Numerical tests of the new model, using injection scenarios with typical parameter sets, show excellent behavior of the new approach for homogeneous geologic formations.

1. Introduction

Geological sequestration of carbon dioxide (CO_2) has been proposed as a promising mitigation strategy to reduce the global warming effects caused by increasing anthropogenic CO_2 emissions [*Benson et al*., 2005]. Such technology involves capturing anthropogenic CO_2 and injecting the captured carbon into permeable geologic formations deep in the subsurface. One important type of storage formation is deep saline aquifers, where CO_2 would be injected into a formation whose pore space is initially filled with brine. In order to effectively mitigate the global warming problem, geological sequestration of CO_2 has to be deployed at a very large scale, with injection increasing to on the order of 3.5 billion tons of carbon per year over the next 50 years [*Pacala and Socolow*, 2004]. With such large amounts of fluids being injected, a range of engineering questions have to be answered to determine if the CO_2 will be stored safely over a long period of time. These questions include the spatial extent of the CO_2 plume, the spatial extent of significant pressure perturbations, and the risk of fluid leakage out of the target formation. To address these issues, mathematical models representing the physical processes of the system are required.

Injection of CO_2 into a saline aquifer leads to a flow system with multiple fluid phases, which typically involves an invading less viscous and less dense supercritical CO_2 phase and a resident more viscous and denser brine phase. Mathematical models for the multiphase flow system vary across a broad range of complexity, from simplified analytical solutions [*Dentz and Tartakovsky*, 2009; *Hesse et al*., 2008, 2007; *Huppert and Woods*, 1995; *Juanes et al*., 2010; *Lyle et al*., 2005; *Nordbotten and Celia*, 2006; *Nordbotten et al*., 2005; *Vella and Huppert*, 2006; *Woods and Mason*, 2000] to full three-dimensional multiphase multicomponent models, such as ECLIPSE [*Schlumberger*, 2010], TOUGH2 [*Pruess*, 2005], STOMP [*White and Oostrom*, 1997], and FEHM [*Zyvoloski et al*., 1997]. One family of simplified models has been developed based on the assumption of vertical equilibrium (VE) [*Dentz and Tartakovsky*, 2009; *Gasda et al*., 2009, 2011, 2012b; *Hesse et al*., 2008, 2007; *Huppert and Woods*, 1995; *Juanes et al*., 2010; *Lyle et al*., 2005; *Nordbotten and Celia*, 2006; *Nordbotten et al*., 2005; *Nordbotten and Celia*, 2012; *Vella and Huppert*, 2006; *Woods and Mason*, 2000]. The VE assumption states that brine and CO_2 segregate instantaneously and are therefore at equilibrium in the vertical direction (i.e., the pressure distribution for each fluid is essentially hydrostatic). This assumption implies that the functional form of the phase pressures in the vertical direction is known, a priori. Therefore, the solution in the vertical does not need to be computed, so that the governing equations for the system are integrated across the vertical direction, resulting in a set of equations defined in the horizontal plane.

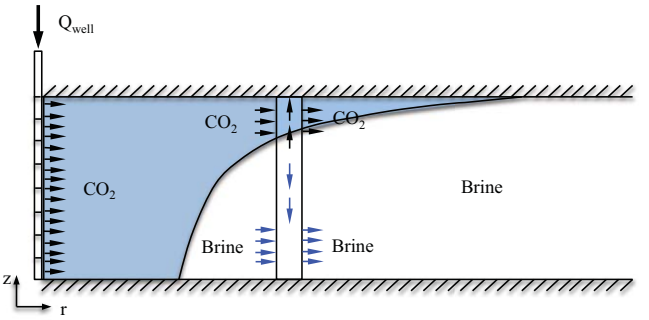

Figure 1. A schematic description of CO_2 injection in an aquifer in the r-z cross section, where a vertical CO_2 injection well is placed on the left side (r = 0) and a vertical column is highlighted to demonstrate flow dynamics of CO_2 and brine. The arrows represent flow directions of the two fluid phases.

The reduction of spatial dimensions gives significant computational advantages over full three-dimensional models. Such VE models are applicable whenever the VE assumption is satisfied. These kinds of models have been used to study many problems related to geological storage of CO_2 [*Bandilla et al*., 2012; *Court et al*., 2012; *Gasda et al*., 2009, 2011, 2012a; *Nilsen et al*., 2011]. However, there are a number of cases (see, for example, [*Court et al*. 2012]) for which the VE assumption is inappropriate. For example, for target formations with relatively low vertical permeability, large formation thickness or small density contrast between CO_2 and brine, the two fluid phases may not reach vertical equilibrium for a long period of time. For problems where the VE assumption is not appropriate, vertical dynamics of CO_2 and brine flow should be included in the models. At present, this means use of full three-dimensional models for the multiphase system.

Here we propose a new model that maintains the computational efficiencies of a vertically integrated model while relaxing the assumption of vertical equilibrium. We cast the new model in a multiscale framework, in direct analogy to the recent presentations of VE models (see, for example, *Nordbotten and Celia* [2012]). The coarse scale is the horizontal domain while the fine scale is the vertical domain, which corresponds to the thickness of the formation. Because the formation thickness is usually much smaller than the horizontal extent, scale separation is appropriate. As in VE models, a vertically integrated equation is solved for the pressure defined at the coarse scale. However, in contrast to VE models that solve a second vertically integrated equation for the vertically integrated phase saturation, followed by analytical reconstruction of the pressure profiles in the vertical direction, the new algorithm solves locally one-dimensional (vertical) dynamic equations to calculate the vertical transients of the fluid saturation profiles. In these locally one-dimensional equations, fine-scale horizontal fluxes are included as sources and sinks. These fine-scale horizontal fluxes are computed from the reconstructed vertical fine-scale pressure field. The pressure reconstruction is based on the coarse-scale pressure and the vertical structure of the fine-scale pressure field from the previous time step. After computing the vertical (fine-sale) saturation, an updated fine-scale pressure is reconstructed. The end result is an algorithm that maintains the computational efficiency of a vertically integrated pressure equation while capturing the vertical dynamics of the two-phase flow system.

In this paper, we provide details and initial computational results for the new algorithm. We first give a brief overview of the basic two-phase flow equations for the CO_2 storage system. This is followed by a brief review of VE models. We then give a presentation of the new multiscale algorithm that incorporates the vertical dynamics into the vertically integrated framework. Next, we compare the new multiscale model with a full multidimensional model and a VE model to demonstrate its applicability under different conditions. Finally, we summarize the key findings and discuss future extensions and directions.

2. Background

The system of CO_2 storage involves a multiphase flow system, which requires a set of equations to represent the flow dynamics of each phase. In this section, we will first introduce the basic equations for the multiphase flow system and then review the VE models that approximate the system as two dimensional by assuming hydrostatic pressure profiles for both phases.

2.1. Two-Phase Flow Equations

Injection of CO_2 into deep saline aquifers usually leads to a two-phase flow system with the fluids being brine and a CO_2-rich phase. Figure 1 depicts the flow dynamics of injected CO_2 and resident brine, both of which have significant horizontal velocities because of the imposed pressure gradient. In addition, the

injected CO_2 will move upward driven by buoyancy whereas the resident brine will experience gravity drainage.

The two-phase flow system can be described by a mass conservation equation for each phase. For simplicity, here we do not consider the mutual solubility of the two fluids, that is, the CO_2-rich phase only contains CO_2 and the brine phase only contains brine. Typically, the mass fraction of the CO_2 component in water under typical pressures and temperatures of geological formations is small (a few percent or less), while the mass fraction of H_2O in the CO_2 phase is even smaller, less than 1% [*Nordbotten and Celia*, 2012]. We note that mutual solubility might be important under certain conditions, e.g., CO_2 dissolution into brine may lead to convective mixing in the vertical direction at large time scales, which may impact CO_2 migration significantly. However, we chose not to include mutual solubility and CO_2 density variations for now, because this paper only focuses on CO_2 injection, the time scale of which is typically short relative to the time scale for convective mixing. The mass balance equation for each fluid phase is given by

$$\frac{\partial}{\partial t}(\rho_\alpha \phi s_\alpha)+\nabla\cdot(\rho_\alpha \mathbf{u}_\alpha)=\rho_\alpha \psi^\alpha, \tag{1}$$

where $\alpha=b$ or c, with b and c representing brine and CO_2, respectively, ϕ is the porosity of the rock, ρ_α is fluid density, s_α is phase saturation, $\mathbf{u}_\alpha$ is the volumetric flux vector, and ψ^α is a source or sink term.

The volumetric flux is governed by the two-phase extension of Darcy's Law

$$\mathbf{u}_\alpha=-\frac{k_{r,\alpha}\mathbf{k}}{\mu_a}(\nabla p_\alpha-\rho_\alpha \mathbf{g}), \tag{2}$$

where $k_{r,\alpha}$ is the relative permeability, $\mathbf{k}$ is the intrinsic permeability tensor, μ_α is viscosity of phase α, p_α is phase pressure, and $\mathbf{g}$ is the gravity acceleration vector.

The relative permeability $k_{r,\alpha}$ is usually approximated as an empirical function of phase saturation. The pressure difference between the two phases is defined as the capillary pressure, which is also commonly parameterized as an algebraic function of phase saturation. That is, we have

$$k_{r,\alpha}=k_{r,\alpha}(s_\alpha), \quad p_c-p_b=p^{cap}=p^{cap}(s_\alpha).$$

Because the pore space must be occupied by either CO_2 or brine, the saturation of the two fluid phases must sum to unity,

$$s_b+s_c=1. \tag{3}$$

The above equations form a closed set of equations for the two-phase flow system of CO_2 storage. To study the CO_2 migration and pressure perturbation during and after injection, we need to solve the two-phase flow equations either analytically or numerically.

2.2. Vertically Integrated Approach With Static (Dupuit) Reconstruction (Vertical Equilibrium)

In this section, we will give a brief overview of VE models. These models assume that the two fluid phases have fully segregated due to buoyancy, and that the phase pressures have reached gravity-capillary equilibrium in the vertical direction. With this assumption, the functional form of the pressure distribution is known, a priori, in the vertical direction. Given the two phase pressures, the capillary pressure function $p^{cap}(s_\alpha)$ can be inverted to give the associated saturation profile in the vertical. Therefore, no numerical solution is needed in the vertical, and it is natural to integrate the governing equations over the thickness of the formation to derive a two-dimensional equation set. The VE algorithm proceeds with numerical solution of the two-dimensional vertically integrated equations and an algebraic (analytical) reconstruction of the vertical profiles based on the VE assumption. This provides a solution for the entire three-dimensional system. We refer to this reconstruction in the vertical as a "static" reconstruction, because no dynamics are included in the vertical dimension. We summarize the VE equations in the following.

Figure 2 is a schematic diagram of the aquifer system, where x_3 is the direction orthogonal to the dominant plane of the formation. All "vertical" integrations are performed along the x_3 direction. Integration of the general three-dimensional equation (1) from the bottom to the top of the aquifer yields

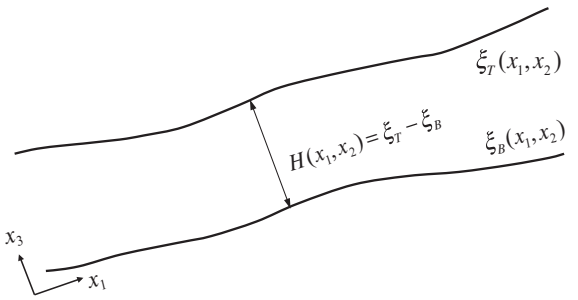

Figure 2. A schematic diagram of the aquifer system. ξ_T and ξ_B are the top and bottom boundary surfaces of the formation, respectively, and $H(x_1, x_2)$ is the thickness of the aquifer.

$$\int_{\xi_B}^{\xi_T}\left(\frac{\partial}{\partial t}(\rho_\alpha\phi s_\alpha)+\nabla\cdot(\rho_\alpha\mathbf{u}_\alpha)\right)dx_3=\int_{\xi_B}^{\xi_T}\rho_\alpha\psi^\alpha dx_3. \tag{4}$$

When the spatial derivative of density can be assumed to be negligibly small, a "slight compressibility" assumption is introduced for the system: this involves keeping the time derivative terms for density and porosity while neglecting the spatial derivatives of density. This is consistent with many models for subsurface flows [*Bear*, 1972; *Gasda et al*., 2009; *Nordbotten and Celia*, 2012]. The standard definitions for compressibilities are given below in equation (5) and (6).

$$d\rho_\alpha=\frac{d\rho_\alpha}{dp}dp=\rho_\alpha c_\alpha dp, \tag{5}$$

$$d\phi=\frac{d\phi}{dp}dp=c_\phi dp, \tag{6}$$

where $c_\alpha=\frac{1}{\rho_\alpha}\frac{d\rho_\alpha}{dp}$ and $c_\phi=\frac{d\phi}{dp}$ are the compressibility coefficients of the fluid phases and the rock, respectively, which are assumed to be constants.

The following vertically integrated variables are defined

$$\Phi(x_1,x_2)\equiv\int_{\xi_B}^{\xi_T}\phi(x_1,x_2,x_3)dx_3,\quad S_\alpha(x_1,x_2,t)\equiv\frac{1}{\Phi}\int_{\xi_B}^{\xi_T}\phi(x_1,x_2,x_3)s_\alpha(x_1,x_2,x_3,t)dx_3,$$

$$\mathbf{U}_\alpha\equiv\int_{\xi_B}^{\xi_T}\mathbf{u}_{\alpha,//}dx_3,\quad \psi^\alpha_{\text{source/sink}}\equiv\int_{\xi_B}^{\xi_T}\psi^\alpha dx_3,\quad \mathbf{K}\equiv\int_{\xi_B}^{\xi_T}\mathbf{k}_{//}dx_3,\quad \Lambda_\alpha\equiv\mathbf{K}^{-1}\int_{\xi_B}^{\xi_T}\mathbf{k}_{//}\lambda_\alpha dx_3,$$

where subscript "//" stands for the (x_1, x_2) plane, and λ_α is the mobility of phase α which is the ratio of relative permeability to fluid viscosity.

The integrals of equation (4) with the substitution of equation (5) in the time derivative term yield

$$\int_{\xi_B}^{\xi_T}\frac{\partial}{\partial t}(\rho_\alpha\phi s_\alpha)dx_3=\rho_\alpha\frac{\partial}{\partial t}(\Phi S_\alpha)+\rho_\alpha c_\alpha\Phi S_\alpha\frac{\partial P_\alpha}{\partial t},$$

$$\int_{\xi_B}^{\xi_T}\nabla\cdot(\rho_\alpha\mathbf{u}_\alpha)dx_3=\rho_\alpha\left[\nabla_{//}\cdot\mathbf{U}_\alpha+\psi^\alpha_T-\psi^\alpha_B\right],$$

where we have used coarse-scale pressure, P_α, to represent the time rate of change of pressure along the x_3 direction. The coarse-scale pressure, P_α, is defined as the pressure of phase α at a reference elevation, taken here to be the elevation of the bottom boundary of the formation, $x_3=\xi_B$, while ψ^α_T and ψ^α_B refer to the fluxes at the top and the bottom, respectively. It should be noted that lower-case variables represent fine-scale variables, while upper-case letters represent coarse-scale variables. The coarse-scale variables, which are defined in the context of vertical integration, can be obtained by either vertical averaging or sampling at one point in the vertical [*Nordbotten and Celia*, 2012], e.g., the coarse-scale saturation, S_α, and mobility, Λ_α, are defined by vertical averaging, while the coarse-scale pressure, P_α, is defined to be the reference pressure at the aquifer bottom.

Because of the VE assumption, the phase pressures are assumed to be hydrostatic:

$$p_\alpha(x_1,x_2,x_3,t)=P_\alpha(x_1,x_2,t)+\rho_\alpha(\mathbf{g}\cdot\mathbf{e}_3)x_3, \tag{7}$$

where $\mathbf{e}_3$ is the unit vector in x_3 direction (assumed to be positive upward).

With these definitions, equation (4) yields the vertically integrated mass balance equation

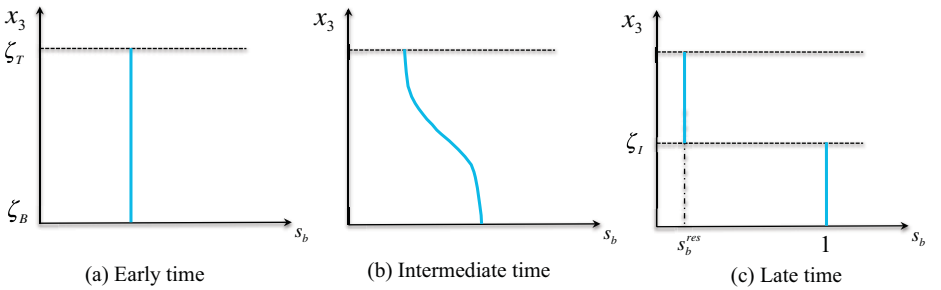

Figure 3. Conceptual evolution of the vertical brine saturation distribution: (a) early time, (b) intermediate time, and (c) late time.

$$\frac{\partial(\Phi S_\alpha)}{\partial t} + c_\alpha \Phi S_\alpha \frac{\partial P_\alpha}{\partial t} + \nabla \cdot \mathbf{U}_\alpha = \Psi^\alpha_{\text{source/sink}} - \psi^\alpha_T + \psi^\alpha_B = \Psi^\alpha. \tag{8}$$

The integrated flux in equation (8) is

$$\mathbf{U}_\alpha = -\mathbf{K}\Lambda_\alpha \cdot (\nabla_{/\!/} P_\alpha - \rho_\alpha \mathbf{G}), \tag{9}$$

where $\mathbf{G} = \mathbf{e}_{/\!/} \cdot \mathbf{g} + (\mathbf{g} \cdot \mathbf{e}_3)\nabla_{/\!/}\xi_B$ and $\mathbf{e}_{/\!/} = (\mathbf{e}_1, \mathbf{e}_2)^T$.

Based on $k_{r,\alpha}(s_\alpha)$ and $p^{cap}(s_\alpha)$, the vertically integrated mobility and capillary pressure can also be related to the vertically integrated saturation algebraically, such that $\Lambda_\alpha = \Lambda_\alpha(S_\alpha)$, $\hat{P}_c - P_b = P^{cap}(S_\alpha)$. The coarse-scale capillary pressure, P^{cap}, is a "pseudocapillary pressure," which is defined as the difference between the coarse-scale pressures. Those pressures are, by definition, the phase pressures evaluated at the bottom of the formation; we use the notation $\hat{P}_c$ to denote the hydrostatic extension of the CO_2 phase pressure evaluated at the bottom of the formation, given that for many locations the CO_2 phase will not be present at the bottom boundary (ζ_B). When neglecting capillary pressure, the functions $\Lambda_\alpha(S_\alpha)$ and $P^{cap}(S_\alpha)$ are linear and simple to derive. A detailed derivation of these two functions can be found in [*Nordbotten and Celia*, 2012]. Although these functions become nonlinear when capillary pressure is included, they can be derived in an analogous way.

The vertically integrated phase saturations also sum to unity.

$$S_c + S_b = 1 \tag{10}$$

By solving the vertically integrated two-dimensional equations, we can compute the vertically integrated saturation and one of the bottom phase pressures, both of which are coarse-scale variables. The pressure and saturation profiles along the vertical direction, which represent the fine scale of the problem, can then be reconstructed algebraically based on the VE assumption.

The applicability of VE models depends on the time scale of fluid segregation (t_s) compared to the simulation time T. If the segregation time is small relative to T, then vertical equilibrium is usually a good approximation; otherwise the VE assumption is not applicable. The segregation time scale can be estimated from

$$t_s \sim \frac{H\phi\mu_b}{k_{r,b,\text{fine}} k_z \Delta\rho g}, \tag{11}$$

where H is formation thickness, μ_b is brine viscosity, $k_{r,b,\text{fine}}$ is the fine-scale relative permeability of brine, k_z is vertical permeability of the formation, $\Delta\rho$ is the density difference between CO_2 and brine, g is the magnitude of gravity acceleration.

To conceptually illustrate the process of reaching vertical equilibrium, we consider the injection of CO_2 into an aquifer through a vertical well that fully penetrates the aquifer. Three schematic plots of the brine saturation profile at different times are shown in Figure 3. At early time, the brine is almost uniformly distributed in the vertical direction as CO_2 invades horizontally along the fully penetrating vertical injection well. The CO_2 then moves upward, driven by buoyancy, and brine simultaneously drains downward through the lighter CO_2 driven by gravity. After a certain period of time, which is the time scale of segregation t_s, CO_2

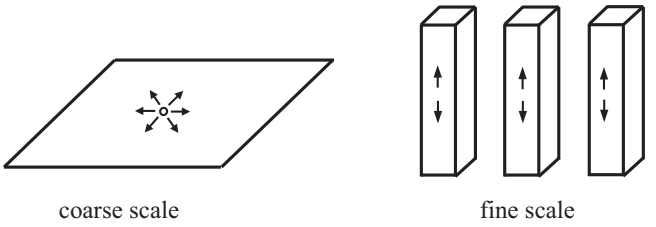

Figure 4. Schematic description of the dynamic reconstruction algorithm: the coarse (horizontal) scale is a two-dimensional domain while the fine scale is represented by a series of one-dimensional (vertical) domains. The arrows indicate the flow of CO_2 and brine, the circle in the coarse scale domain represents the location of the injection well.

and brine segregate essentially completely with CO_2 residing on top of brine. For simplicity, in Figure 3, we have neglected local capillary pressure; therefore, when both CO_2 and brine reach vertical equilibrium, they form a macroscopic sharp interface, ζ_l, as shown in Figure 3c. If $t_s \ll T$, then we can usually neglect the vertical redistribution process and simply assume CO_2 and brine have already segregated; this is the VE assumption. However, when t_s is comparable or even larger than T, we have to include the vertical dynamics of CO_2 and brine in order to accurately predict CO_2 migration.

3. Multiscale Algorithm—Vertical Dynamic Reconstruction

The VE model is accurate and computationally efficient as long as the VE assumption is satisfied. However, such a simplified model will not be applicable when the time scale of fluid segregation is not small relative to the simulation time. In order to extend the applicability of vertically integrated models, we present a multiscale method that relaxes the VE assumption and includes the vertical dynamics of CO_2 and brine, but still uses the vertically integrated framework. We refer to this multiscale method as "dynamic reconstruction," as opposed to static reconstruction in the VE model, because in the new approach flow dynamics are included in the vertical reconstruction. In this section, we first describe the dynamic reconstruction algorithm and then derive the equations for both the coarse and fine scales. We then present the numerical solution procedure that we have implemented.

3.1. Algorithm Overview

The dynamic reconstruction algorithm involves two scales: a coarse scale, which is a vertically integrated two-dimensional domain; and a fine scale that is a one-dimensional domain across the vertical extent of the formation (see Figure 4). The coarse (horizontal) scale is used to solve vertically integrated equations for the coarse-scale pressure, $P_b\,(x_1, x_2, t)$. Given the solution for $P_b\,(x_1, x_2, t)$, the fine (vertical) scale is then solved for the phase saturation, using the fractional-flow form of the governing equation. By using no-flow boundary conditions along the top and bottom boundaries of the formation and horizontal fluxes (estimated from the solution for P_b) as local sources and sinks, the fractional-flow equation can be solved along any line in the x_3 direction $(\xi_B < x_3 < \xi_T)$ for $s_c\,(x_1, x_2, x_3, t)$ as a one-dimensional problem. We then complete the calculations by using both $P_b\,(x_1, x_2, t)$ and $s_c\,(x_1, x_2, x_3, t)$ to analytically reconstruct the phase pressures along the x_3 direction.

3.2. Governing Equations

The set of governing equations for the overall dynamic reconstruction algorithm has two parts: a vertically integrated two-dimensional equation for the coarse-scale pressure, and a set of one-dimensional equations for the fine scale. The coarse-scale equation is formed by summing the integrated mass balance equations for both fluid phases. This summed equation is analogous to the equation used in the VE models; the integrated mass balance equations are given already in equation (8), and the summed equation takes the following form,

$$\left(c_\phi H + c_b \Phi\right) S_b \frac{\partial P_b}{\partial t} + \left(c_\phi H + c_c \Phi\right) S_c \frac{\partial P_c}{\partial t} + \nabla_{/\!/} \cdot \left(\mathbf{U}_b + \mathbf{U}_c\right) = \Psi^b + \Psi^c, \tag{12}$$

where the coarse-scale variables are as defined in section 2. Note that the coarse-scale mobilities in the dynamic reconstruction model have the same definition as in the VE model, but they have to be numerically integrated from the fine-scale mobilities and they will hence differ from the VE case. The definition of coarse-scale capillary pressure is also different from the VE algorithm; it is locally defined instead of being the "pseudocapillary pressure" as in the VE model.

To this point, the procedure is almost identical to the vertical equilibrium approach, the differences being in the details of the coarse-scale coefficients as described above. However, as shown in equation (7), the VE approach imposes a strict hydrostatic condition on both phase pressures, which serves to define the pressure structure used in the definition of integrated fluxes $\mathbf{U}_b$ and $\mathbf{U}_c$. The VE pressure distribution is inappropriate in the new algorithm, except in the limits where VE is applicable. Therefore, in the dynamic reconstruction, we use a more general pressure reconstruction. In the spirit of equation (7), we write a generalized pressure function as

$$p_\alpha(x_1, x_2, x_3, t) = P_\alpha(x_1, x_2, t) + \pi_\alpha(x_1, x_2, x_3, t). \tag{13}$$

In this equation, the function π_α defines the vertical fine-scale reconstruction of the pressure field for phase α. Specific choices for this reconstruction function are discussed later in this section. With this reconstructed pressure, the integrated fluxes can be calculated by computing the gradient in the x_1 and x_2 directions of the function p_α. Equation (12) can then be solved for a coarse-scale pressure, which can be chosen as either P_b or P_c or any combination of these two pressures. P_b is chosen in this paper. Details of the numerical solution algorithm are given in section 3.3.

In the fine-scale model, the phase mass balance equations are rearranged to focus on the vertical dynamics. The fine-scale mass balance for each phase can be written as follows,

$$\frac{\partial(\rho_\alpha \phi s_\alpha)}{\partial t} + \frac{\partial(\rho_\alpha u_{\alpha,3})}{\partial x_3} = \rho_\alpha \psi^\alpha - \nabla_{//} \cdot \left(\rho_\alpha \mathbf{u}_{\alpha,//}\right), \tag{14}$$

where $u_{\alpha,3}$ is the flux of fluid phase α in the x_3 direction, and $\mathbf{u}_{\alpha,//}$ is the flux in the (x_1, x_2) plane which will be estimated from the solution of equations (12) and (13) by using equation (15),

$$\mathbf{u}_{\alpha,//} = -\mathbf{k}_{//} \lambda_\alpha \cdot [\nabla_{//} p_\alpha - \rho_\alpha (\mathbf{e}_{//} \cdot \mathbf{g})]. \tag{15}$$

Again as in the vertical equilibrium case, we assume "slight compressibility," leading to

$$\phi \frac{\partial s_\alpha}{\partial t} + (c_\phi + \phi c_\alpha) s_\alpha \frac{\partial p_\alpha}{\partial t} + \frac{\partial u_{\alpha,3}}{\partial x_3} = \psi^\alpha - \nabla_{//} \cdot \mathbf{u}_{\alpha,//}. \tag{16}$$

Equation (16) is summed over the two phases, and the resulting equation is used to estimate the total flux, $u_{\mathrm{TOT},3}$ in the x_3 direction, where $u_{\mathrm{TOT},3} = u_{b,3} + u_{c,3}$. Given the total flux values in the x_3 direction, the vertical phase flux $u_{\alpha,3}$ can be calculated using the fractional-flow form of Darcy's Law, which takes the following form,

$$\begin{aligned} u_{b,3} &= f_b \cdot \left(u_{\mathrm{TOT},3} - k_3 \lambda_c \Delta\rho g + \lambda_c k_3 \frac{\partial p^{cap}}{\partial x_3} \right) \\ u_{c,3} &= f_c \cdot \left(u_{\mathrm{TOT},3} + k_3 \lambda_b \Delta\rho g - \lambda_b k_3 \frac{\partial p^{cap}}{\partial x_3} \right), \end{aligned} \tag{17}$$

where k_3 is permeability in x_3 direction, and f_α is the fractional-flow function, given by

$$f_\alpha = \frac{\lambda_\alpha}{\lambda_b + \lambda_b}.$$

At this point, all the vertical and horizontal phase fluxes are known, allowing us to compute (reconstruct) the phase saturations using equation (16).

Finally, we return to the issue of pressure reconstruction on the fine scale (equation (13)). We seek a pressure reconstruction function that is simple to compute, is physically motivated, and produces the VE model at the appropriate limits. After experimenting with a number of choices, our current preferred choice is the following saturation-weighted pressure functions for the two phases:

$$\begin{aligned} \frac{\partial p_c}{\partial x_3} &= -(s_c \rho_c + s_b \rho_b) g + s_b \frac{\partial p^{cap}(s_b)}{\partial x_3} \\ \frac{\partial p_b}{\partial x_3} &= -(s_c \rho_c + s_b \rho_b) g - s_c \frac{\partial p^{cap}(s_b)}{\partial x_3}. \end{aligned} \tag{18}$$

From equation (18), the function π_α in equation (13) can be derived. For example, when $\alpha = b$, integration from the bottom of the formation yields

$$p_b(x_1,x_2,x_3,t)=P_b(x_1,x_2,t)-\int_{\xi_B}^{x_3}\left[(s_c\rho_c+s_b\rho_b)g+s_c\frac{\partial p^{cap}(s_b)}{\partial x_3}\right]dx_3. \tag{19}$$

It should be noted that the reconstructed fine-scale pressure is only used to compute horizontal fine-scale fluxes, and is not directly used in the vertical flux calculation. Thus, the appropriateness of the pressure reconstruction only depends on how well it captures the horizontal fine-scale fluxes. There are three forces that drive the horizontal flow: the viscous force, capillary pressure, and buoyancy. Different forces become dominant in different regimes or periods. For the regime that is close to the injection well or before CO_2 and brine segregate, viscous forces dominate. For the regime that is far from the injection well, or after CO_2 and brine segregate, capillary pressure and gravity forces become dominant. The pressure reconstruction should be able to capture the evolution of the dominant forces. Any reconstruction that has the coarse-scale pressure included can approximately capture the viscous forces when viscous forces are dominant, while the saturation-weighted hydrostatic pressure profile is currently the only reconstruction we have developed that not only accounts for the viscous forces, but also captures the capillary pressure and buoyancy when these two forces become dominant. Other options could be chosen, for example, instead of using the fine-scale reconstructed pressure field, the coarse-scale horizontal pressure gradient can be used to compute the fine-scale fluxes (that is, apply the coarse pressure gradient along the entire vertical). This option gives good results when CO_2 and brine are not segregated, meaning it captures the viscous forces well, but it induces significant errors when CO_2 and brine segregate and reach vertical equilibrium in some cases. This is simply because when CO_2 and brine are in equilibrium, fine-scale pressure gradient is different from the coarse-scale pressure gradient and that difference is largely due to capillary pressure and buoyant force. Other choices may be explored for the pressure reconstruction, but our results to date indicate that the saturation-weighted reconstruction gives good results.

3.3. Numerical Solution Procedure

To solve the dynamic reconstruction model numerically we discretize space by using a standard cell-centered finite-volume method. For the time discretization, we use a scheme analogous to the implicit pressure and explicit saturation (IMPES) method: an implicit treatment of the pressure at the coarse scale and an explicit treatment of saturation at the fine-scale decouples the two scales. Hence, we are able to first solve the coarse-scale pressure implicitly and then calculate the fine-scale saturations explicitly. Details of the algorithm implementation are presented in this section. For the sake of clarity, we use continuous operators in space in our exposition.

The time-discrete version of equation (12) with implicit brine pressure P_b and explicit treatment of saturations is given by

$$\begin{aligned}&\left(c_\phi H+c_b\Phi S_b^n+c_c\Phi S_c^n\right)\frac{P_b^{n+1}-P_b^n}{\Delta t}+\left(c_\phi H+c_c\Phi\right)S_c^n\frac{P^{cap,n}-P^{cap,n-1}}{\Delta t}\\ &-\nabla_{/\!/}\cdot\left\{\mathbf{K}[(\Lambda_b^n+\Lambda_c^n)\cdot\nabla_{/\!/}P_b^{n+1}+\Lambda_c^n\nabla_{/\!/}P^{cap,n}-(\Lambda_b^n\rho_b+\Lambda_c^n\rho_c)(\mathbf{e}_{/\!/}\cdot\mathbf{g})]+\int_{\xi_B}^{\xi_T}\mathbf{k}_{/\!/}\left(\lambda_b^n\nabla_{/\!/}\pi_b^n+\lambda_c^n\nabla_{/\!/}\pi_c^n\right)dx_3\right\}.\\ &=\Psi^{b,n+1}+\Psi^{c,n+1}.\end{aligned} \tag{20}$$

where superscript n stands for the discrete time level t^n and $n+1$ stands for t^{n+1}. This is a linear equation for the coarse-scale pressure P_b^{n+1} at time t^{n+1} that can be solved by a sparse matrix solver.

For the fine-scale transport of the saturations using equation (16), we first calculate the horizontal phase fluxes as follows

$$u_{\alpha,/\!/}^{n+1,*}=-\mathbf{k}_{/\!/}\lambda_\alpha^n\cdot\left[\nabla_{/\!/}p_\alpha^{n+1,*}-\rho_\alpha(\mathbf{e}_{/\!/}\cdot\mathbf{g})\right]. \tag{21}$$

where $p_\alpha^{n+1,*}(x_1,x_2,x_3)=P_\alpha^{n+1}(x_1,x_2)+\pi_\alpha^n(x_1,x_2,x_3)$, and the superscript * denotes that the variable is an approximation at time t^{n+1}.

The horizontal total flux $u_{\mathrm{TOT},/\!/}^{n+1,*}=u_{b,/\!/}^{n+1,*}+u_{c,/\!/}^{n+1,*}$ is then used to calculate the vertical total flux from the time-discrete version of equation (16) summed over the two phases, that is

$$\frac{\partial u_{\mathrm{TOT},3}^{n+1,*}}{\partial x_3}=-\nabla_{/\!/}\cdot\mathbf{u}_{\mathrm{TOT},/\!/}^{n+1,*}+\psi^{b,n+1}+\psi^{c,n+1}-\left(c_\phi+\phi c_b\right)s_b\frac{p_b^{n+1,*}-p_b^n}{\Delta t}-\left(c_\phi+\phi c_c\right)s_c\frac{p_c^{n+1,*}-p_c^n}{\Delta t}. \tag{22}$$

Table 1. Numerical Solution Procedure of Dynamic Reconstruction Algorithm

Given the initial value of pressure p^0 and saturation s_α^0:
For all discrete time steps n = 0, 1, . . ., N **do**
  Compute λ_α^n and Λ_α^n, solve for P_b^{n+1};
  Assume $p_\alpha^{n+1,*} = P_\alpha^{n+1} + \pi_\alpha^n$, compute $\mathbf{u}_{\alpha,//}^{n+1,*}$ and $\mathbf{u}_{\mathrm{TOT},//}^{n+1,*}$;
  Compute $u_{\mathrm{TOT},3}^{n+1,*}$ and $u_{\alpha,3}^{n+1,*}$;
  Compute s_α^{n+1}, analytically reconstruct p_α^{n+1}.
End for

With the vertical total flux $u_{\mathrm{TOT},3}^{n+1,*}$ and no-flow boundary conditions at the top and bottom of the formation, we obtain the phase fluxes with the time-discrete version of equation (17) given by

$$\begin{aligned} u_{b,3}^{n+1,*} &= f_b^n \cdot \left(u_{\mathrm{TOT},3}^{n+1,*} - k_3 \lambda_c^n \Delta\rho g + \lambda_c^n k_3 \frac{\partial p^{cap,n}}{\partial x_3} \right) \\ u_{c,3}^{n+1,*} &= f_c^n \cdot \left(u_{\mathrm{TOT},3}^{n+1,*} + k_3 \lambda_b^n \Delta\rho g - \lambda_b^n k_3 \frac{\partial p^{cap,n}}{\partial x_3} \right). \end{aligned} \tag{23}$$

Then the saturations s_α^{n+1} can be computed explicitly using the time-discrete version of equation (16) that reads as

$$\phi \frac{s_\alpha^{n+1} - s_\alpha^n}{\Delta t} + (c_\phi + \phi c_\alpha) s_\alpha \frac{p_\alpha^{n+1,*} - p_\alpha^n}{\Delta t} + \frac{\partial u_{\alpha,3}^{n+1,*}}{\partial x_3} = \psi^{\alpha,n+1} - \nabla_{//} \cdot \mathbf{u}_{\alpha,//}^{n+1,*}. \tag{24}$$

Finally, we obtain the updated pressure field in the vertical direction as

$$\begin{aligned} p_b^{n+1} &= P_b^{n+1} - \int_{\xi_B}^{x_3} \left[(s_c^{n+1}\rho_c + s_b^{n+1}\rho_b) g + s_c^{n+1} \frac{\partial p^{cap}(s_b^{n+1})}{\partial x_3} \right] dx_3 \\ p_c^{n+1} &= P_b^{n+1} + P^{cap,n+1} - \int_{\xi_B}^{x_3} \left[(s_c^{n+1}\rho_c + s_b^{n+1}\rho_b) g - s_b^{n+1} \frac{\partial p^{cap}(s_b^{n+1})}{\partial x_3} \right] dx_3 \end{aligned} \tag{25}$$

The solution procedure is summarized in table 1.

4. Results

In this section, we present results from the dynamic reconstruction model and compare them with results from two other models: a full multidimensional model and a VE model. For simplicity, we compare them in a two-dimensional cross-sectional domain so that the problem setup only has one horizontal dimension and one vertical dimension. The full multidimensional model is therefore a two-dimensional (2D) simulator, which solves the full equations using an IMPES method [*Doster et al.*, 2014]. For most of the test cases, we neglect capillary pressure, so that the VE model is a sharp-interface model. This allows for easy visual comparison of the results. Also, we neglect compressibility for simplicity. Two test scenarios have been designed (Figure 5). The first scenario involves injection through a vertical, fully penetrating well, while the second scenario involves injection from a location at the bottom of the formation. In each scenario, we will present CO_2 plume comparisons for both early times (1∼5 years) and later time (50 years). In the first scenario, we neglect capillary pressure and study two different values of permeability. We expect that the time scale of fluid segregation for the larger permeability (100 mD) is small so that it is consistent with the VE assumption, while with the lower permeability (10 mD) the fluids take a longer time to segregate in which case the VE assumption may be invalid. In the second scenario, we keep the permeability fixed at 10 mD and study the performance of the dynamic reconstruction model for a partially penetrating injection well both with and without capillary pressure.

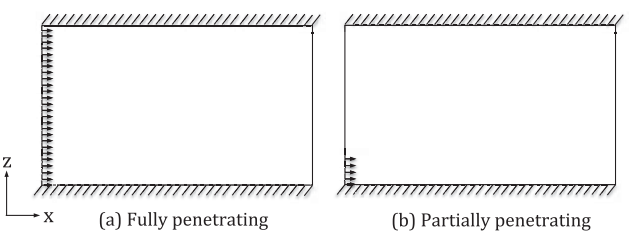

Figure 5. Problem setup for the numerical experiments: (a) fully penetrating case and (b) partially penetrating case.

The problem setup for both scenarios is shown in Figure 5. Top and bottom boundaries are no-flow. Along the left boundary, CO_2 is injected from a well at a constant flow rate. The well spans the entire thickness of the formation in the fully penetrating case, and only the bottom 1 m in the partially penetrating case. Along the right boundary, a flux boundary condition is imposed where we extract, uniformly along the vertical direction, the same mass of fluid as we inject on the left side. The formation is 50 m thick, and the domain size in the x direction depends on different simulation times: a shorter length is chosen for early time simulations to allow use of fine grid spacing. For early time simulations, the domain size is $l_x = 1500$ m, $l_z = 50$ m, and the grid size is $\Delta x = 5$ m, $\Delta z = 0.2$ m; for later time, the domain size is $l_x = 15{,}000$ m, $l_z = 50$ m, and the grid size is $\Delta x = 25$ m, $\Delta z = 0.25$ m. We inject 0.71 kg/s/m (2.24×10^{-4} Mt/yr/m) CO_2 uniformly from the left side, which is equivalent to a 500 m long horizontal well with an injection rate of about 0.2 Mt CO_2 per year. Densities of CO_2 and brine are 710 and 1000 kg/m^3; viscosities are 4.25×10^{-5} and 3.0×10^{-4} Pa s, respectively; porosity of the rock formation is 0.15. We use Brooks-Corey curves for relative permeability and capillary pressure (when capillary pressure is included) with pore size distribution index as 2.0 and entry pressure as 1.0×10^4 Pa.

4.1. CO_2 Plume Comparison for a Fully Penetrating Injection Well

In this section, two cases with fully penetrating injection wells will be presented. The first case involves a formation with relatively low permeability of 10 mD, while the second case has a higher permeability of 100 mD. The time scale of vertical fluid segregation is larger in the low-permeability case than in the high-permeability case, so that the low-permeability case is less favorable for VE models.

In Figures 6, we present comparisons for the case with a permeability of 10 mD. Different rows show results for different simulation times. The top two rows show the CO_2 plumes for the three models for early simulation times, which we take to be the first 5 years after injection begins; the bottom row shows the CO_2 plumes for late times, which we take to be 50 years. We show results for the spatial distribution of the CO_2 (left and middle columns) as well as a comparison of the CO_2 invasion front location for all three models in the right column. From the comparison, we can see that the dynamic reconstruction model is very close to the full two-dimensional model both in terms of the CO_2 distribution and the CO_2 invasion front. The CO_2 invasion front is defined as the transition from grid cells with CO_2 saturation greater than 1% to neighbor cells with saturation less than 1%. The red (white for the third row) dashed line in the left and middle plots represent the CO_2-brine interface from the VE model. In the VE model, CO_2 saturation above the interface is 1 and below it is 0 (no residual saturation considered here). The CO_2 plume from the VE model is different from the other two models and we can see that it tends to overestimate the outer-most extent (or "tip") of the CO_2 front, in fact, the tip of the CO_2 plume has traveled about twice as far as for the VE model, and the shape of the invading fronts remains different even though the fluids are strongly segregated after 50 years. Overall, the match between the dynamic reconstruction model and the full two-dimensional model is excellent, while the VE model is significantly different especially for early times.

The CO_2 plume comparison for the case with 100 mD is shown in Figure 7. For early simulation times, the three models are all very close (see top two rows of Figure 7). If we look at the longer simulation times, they become even closer (see bottom row of Figure 7). The VE assumption appears to work well in this case, and we can see that the three models give similar results, although the VE model still overestimates the tip location somewhat.

4.2. CO_2 Plume Comparison for a Partially Penetrating Injection Well

The second injection scenario is injection through a partially penetrating well, as illustrated in Figure 5b. In this case, CO_2 is injected through the bottom 1m of the aquifer, and the total injection rate is the same as for the fully penetrating case and hence the CO_2 is injected at higher velocity creating a steeper pressure gradient. Because more vertical pressure-driven flow is involved, especially close to the injection well, this is a stronger test of the dynamic reconstruction model, in particular the assumption of a saturation-weighted hydrostatic pressure profile in the pressure reconstruction. Here, we show the results for the case with relatively low permeability (10 mD), since this is the more challenging case for the dynamic reconstruction model. In the 100 mD case (not shown here), we observe very good agreement of the dynamic reconstruction and the full two-dimensional model and all three models are close, similar to what was observed in the fully penetrating case with permeability of 100 mD.

The comparison of the three models for the partially penetrating scenario without capillary pressure is shown in Figure 8. Again, the top two rows are for early simulation times and the bottom row is for late

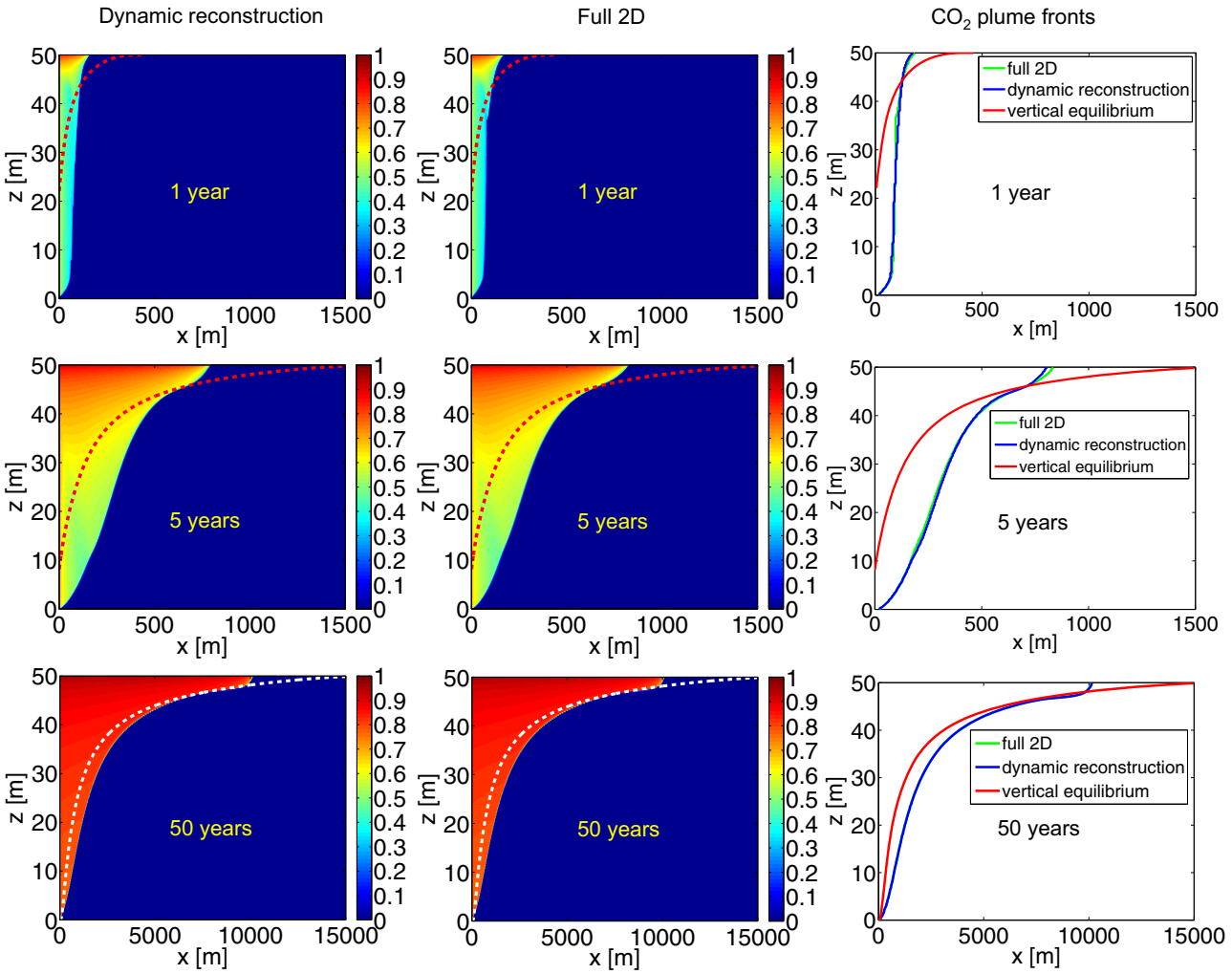

Figure 6. A comparison of the CO_2 plumes for the three models under a fully penetrating injection scenario, with the permeability of the formation being 10 mD and capillarity neglected. The three rows show results at t = 1, t = 5, and t = 50 years, respectively. Note the scale on the *x* axis is 10 times larger in the third row. The left and middle columns show the predicted CO_2 plumes using the dynamic reconstruction model and the full two-dimensional model, respectively. The color indicates the magnitude of CO_2 saturation, while the superimposed red (white for the third row) dashed line shows the CO_2-brine interface from the VE model. The right column shows the location of the CO_2 invasion front for all three models.

simulation time. Despite injecting from the bottom of the aquifer, the results show that the dynamic reconstruction model is still close to the full two-dimensional model. Even the nonmonotonic saturation distribution along horizontal cross sections in the middle of the aquifer (see middle row of Figure 8) is captured well. The only significant difference occurs for the earliest time (i.e., after 1 year injection), where we observe that the dynamic reconstruction model has more CO_2 at the top of the aquifer and that the CO_2 at the top moves slightly further away from the left boundary, as compared with the full two-dimensional model. But, in that case, we can see that the VE model gives much worse results than the dynamic reconstruction model: all of the CO_2 accumulates to the top part of the aquifer due to the VE assumption.

Finally, a CO_2 plume comparison of the three models for a partially penetrating injection scenario with capillary pressure taken into account is shown in Figure 9. Similar to the case without capillary pressure, the dynamic reconstruction shows very good agreement with the full two-dimensional model except at the earliest time (i.e., after 1 year injection). But, again, the VE model gives much worse results than the dynamic reconstruction model in that case. We should note that although the VE model is still quite different from the other two models, it gives better results compared to the case without capillary pressure. In particular, the VE model tends to overestimate the outer-most extent of the CO_2 plume less when capillary pressure is included.

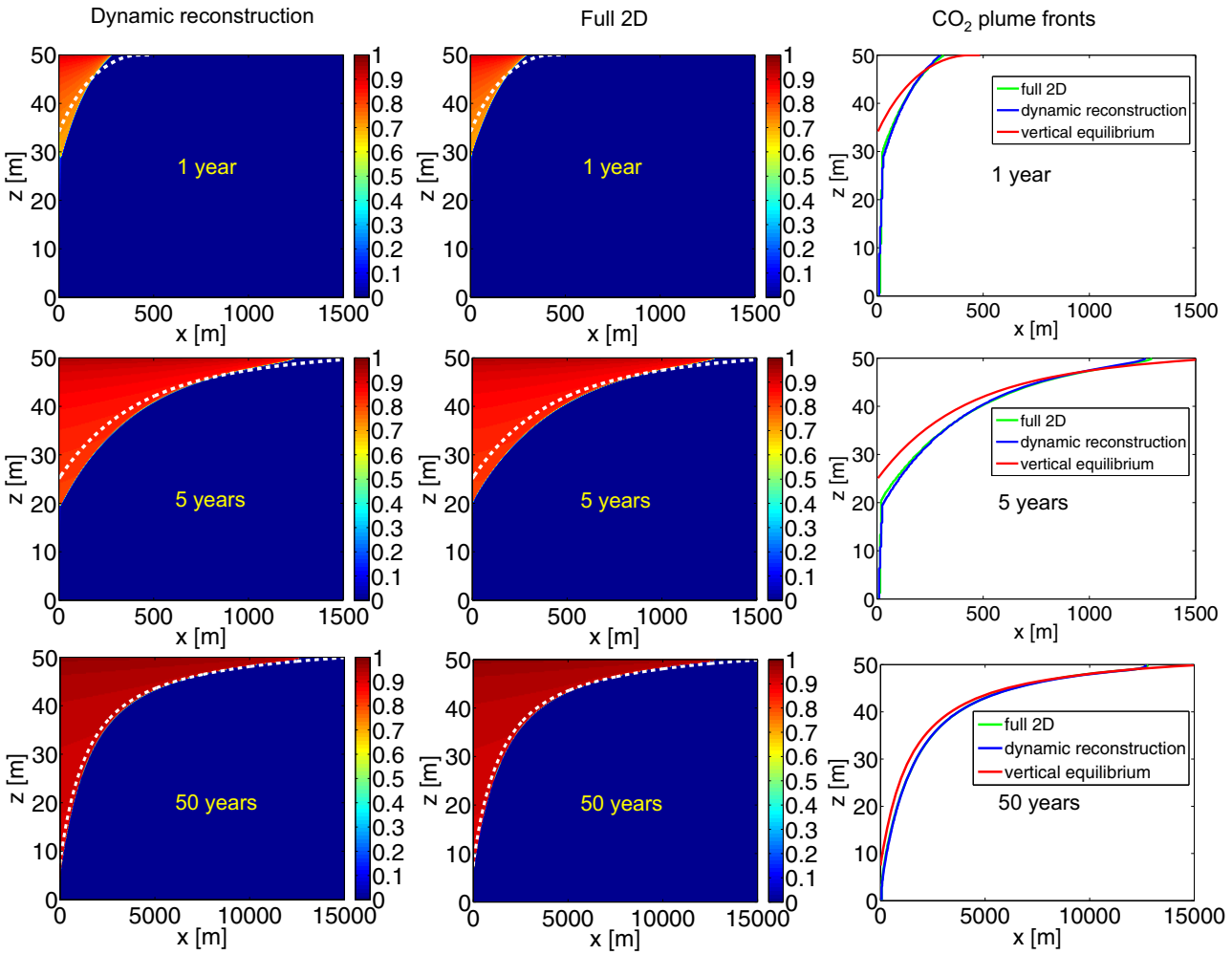

Figure 7. A comparison of the CO_2 plumes for the three models under a fully penetrating injection scenario, with permeability of the formation being 100 mD and capillarity neglected. The three rows show results at t = 1, t = 5, and t = 50 years, respectively. The left and middle columns show the predicted CO_2 plumes using the dynamic reconstruction model and the full two-dimensional model, respectively. The color indicates the magnitude of CO_2 saturation, while the superimposed white dashed line shows the CO_2-brine interface from the VE model. The right column shows the location of the CO_2 invasion front for all three models.

5. Discussion

The model comparisons show that the dynamic reconstruction model agrees very well with the full two-dimensional model for the considered injection scenarios: an injection with a fully penetrating well into a formation with low or high permeability, as well as an injection with a partially penetrating well with or without capillary pressure. In the fully penetrating injection scenario, the dynamic reconstruction model shows excellent agreement with the full two-dimensional model for all simulation times. For the partially penetrating injection scenario, there is some difference between the CO_2 plumes from the dynamic reconstruction model and the full two-dimensional model at early times (i.e., after 1 year injection). This is not surprising, based on our pressure reconstruction method. The reconstructed pressure profile is not used directly in the algorithm, instead only the horizontal pressure gradient is used to compute horizontal fluxes. Such an approximation works very well for the fully penetrating case even if the pressure profile is not hydrostatic. For the fully penetrating well, the horizontal pressure gradient is almost uniformly distributed along the vertical, so that the horizontal pressure gradient calculated from the saturation-weighted hydrostatic pressure profile, which is ultimately based on the pressure gradient at the bottom of the formation, is a good approximation. However, for the partially penetrating case, especially close to the well, pressure-driven flow in the vertical direction is more pronounced leading to a less uniform horizontal pressure

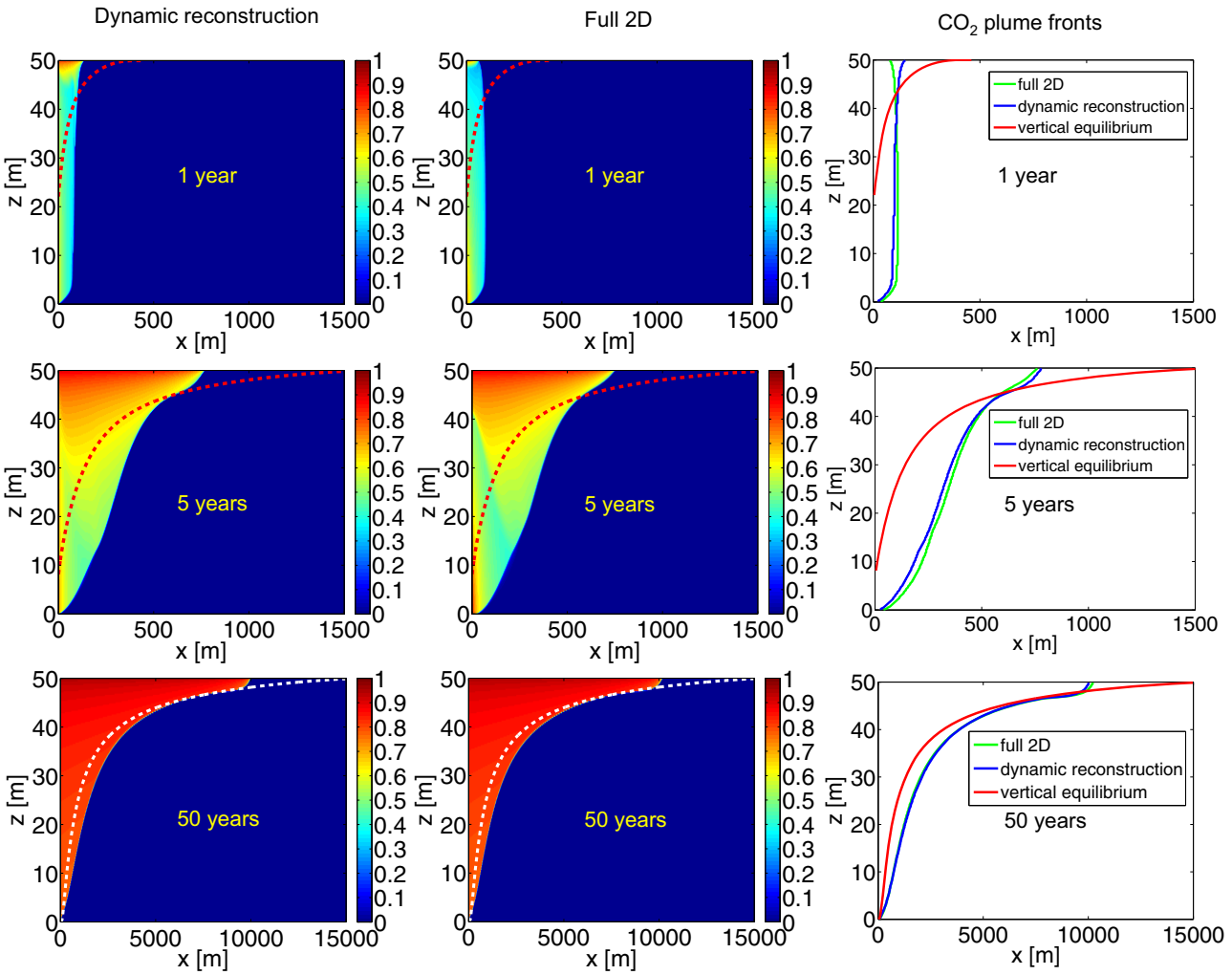

Figure 8. A comparison of the CO_2 plumes for the three models under a partially penetrating injection scenario, with permeability of the formation being 10 mD and capillarity neglected. The three rows show results at t = 1, t = 5, and t = 50 years, respectively. The left and middle columns show the predicted CO_2 plumes using the dynamic reconstruction model and the full two-dimensional model, respectively. The color indicates the magnitude of CO_2 saturation, while the superimposed red (white for the third row) dashed line shows the CO_2-brine interface from the VE model. The right column shows the location of the CO_2 invasion front for all three models.

gradient distribution. In fact, the horizontal pressure gradient at the top may differ significantly from the gradient at the bottom close to the well. Therefore, the reconstructed pressure profile in the dynamic reconstruction model tends to overestimate the horizontal flux at the top of the aquifer, which leads to overestimation of the vertical flux as well. As such, the dynamic reconstruction model overestimates the amount of CO_2 at the top and the location of the tip of the CO_2 plume compared with the full two-dimensional model, especially at early times. It should be noted that, from a regulatory perspective the algorithm can thus be assumed to be conservative, as the CO_2 plume area would be overestimated. However, at later times, even after only 5 years, there is good agreement between the dynamic reconstruction model and the full two-dimensional model. This is because further away from the well the horizontal pressure gradient becomes more uniform along the vertical direction and this renders our pressure approximation more reasonable. Overall, we observe that the dynamic reconstruction appears to give remarkably good agreement with the full two-dimensional model, even for the partially penetrating case, especially at later times.

The dynamic reconstruction model naturally maintains much of the computational efficiency of the VE models because it still uses the vertically integrated framework. The pressure solution, which usually requires the most computational effort in an IMPES-type method, is only solved in two dimensions in the coarse-scale model. The transport solution is decoupled into one-dimensional countercurrent flow in the

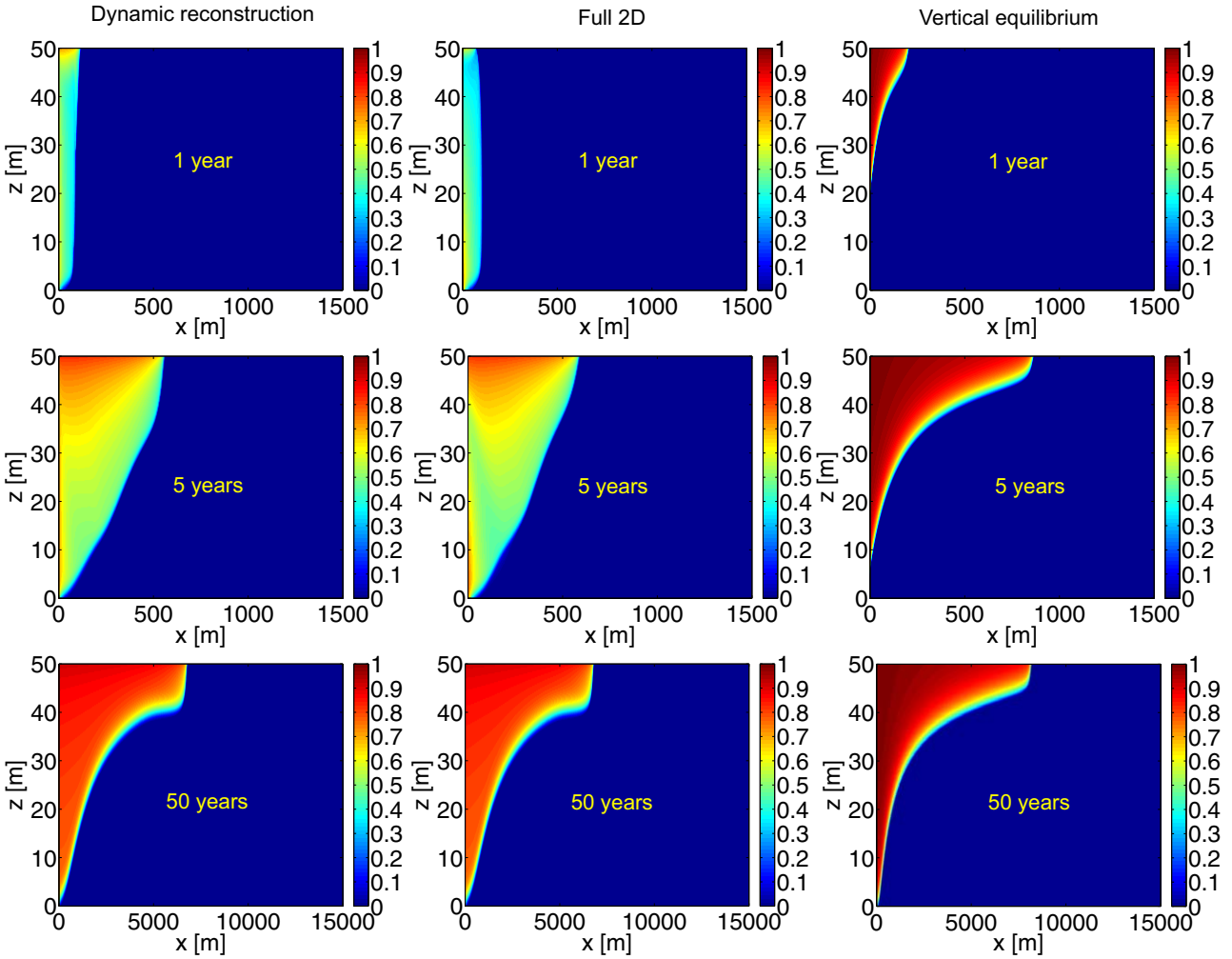

Figure 9. A comparison of the CO_2 plumes for three models under a partially penetrating injection scenario, with the permeability of the formation being 10 mD and capillary pressure included. The three rows show results at t = 1, t = 5, and t = 50 years, respectively. The left, middle, and right columns show the predicted CO_2 plumes using the dynamic reconstruction model, the full two-dimensional model, and the vertical equilibrium model, respectively. The color indicates the magnitude of CO_2 saturation.

vertical and a two-dimensional transport in the horizontal. Therefore, we do solve the transport in three dimensions (explicitly), which in the case of fast vertical segregation may be constrained by a CFL condition that is significantly stricter than for the purely horizontal two-dimensional transport in VE models. This may be remedied by using smaller time steps in the transport calculation compared to the coarse-scale pressure solution. The higher cost of the dynamic reconstruction model, compared to the VE model, also reflects that before the fluids segregate in the vertical, some computational effort must be spent to resolve the vertical flow. Because of the decoupling between the coarse scale and fine scale, we observe the grid sizes Δx andΔz cannot be chosen independently. Smaller ratios of $\Delta z/\Delta x$ give better agreement with the full two-dimensional simulation; based on numerical experimentation, we choose the ratio $\Delta z/\Delta x$ less than unity, often on the order of 0.1. However, we note that since the physical system of CO_2 storage usually has orders of magnitude larger extent in the horizontal than in the vertical direction, the spatial discretization naturally leads to a small grid size ratio $\Delta z/\Delta x$ in order to be computationally practical. In terms of computational efficiency, despite inclusion of more physics, the dynamic reconstruction model only takes about three times of the computational time compared to the VE model per time step even if 200 grid cells are placed along the vertical in the later time simulations. We should note that the time step of the dynamic reconstruction model may be restricted by the fine-scale calculation, but in that case, a different (larger) time step could be chosen for the coarse scale. By comparison with the full two-dimensional model, even if these two algorithms are implemented in different programming languages and using different linear system

solvers, we observe that the dynamic reconstruction model is at least 1 order of magnitude faster for most cases. Overall, this implies that the dynamic reconstruction model captures more physics than the VE models while still maintaining much of the computational advantages over full multidimensional models.

Because the purpose of this paper is to introduce the new dynamic reconstruction algorithm, we have used relatively simple example problems to demonstrate the concept and to show that the algorithm appears to give significant improvements compared to the VE model while retaining many of its attractive features. All of the example problems involve homogeneous, horizontal, isotropic formations with uniform thickness involving two immiscible fluid phases. The design of the algorithm does not explicitly rely on these simplifications. Thus, we expect that inclusion of material heterogeneities, geometric complexities, and phase interactions including dissolution and miscible transport is possible within our general framework. However, we have not implemented those extensions, so their efficacy remains to be studied.

6. Conclusion

A novel multiscale method for modeling CO_2 storage has been presented in this paper, based on vertically integrated equations coupled with a dynamic reconstruction of saturation and pressure in the vertical direction. This differs from the usual vertically integrated models, which assume vertical equilibrium and therefore do not include any vertical flow dynamics. For the example problems studied, the new model shows excellent agreement with full multidimensional models, and shows significant improvements over Vertical Equilibrium (VE) models for cases when vertical equilibrium is not an appropriate assumption. The new model also matches the VE results in the limit of very fast segregation times, which are the cases for which VE is applicable. Overall, the dynamic reconstruction model provides a new multiscale framework for large-scale CO_2 storage problems which extends the scope of applicability of vertically integrated models. Extensions to include additional fine-scale physics, such as vertical heterogeneity and fluid solubility, should also be possible although we have not yet explored these in any depth.

The dynamic reconstruction model maintains many of the computational advantages of the VE model and therefore requires much less computational effort compared to full multidimensional models. The ability to capture more physics while still maintaining a low level of computational effort makes these dynamic reconstruction models attractive for computational studies of large-scale CO_2 storage systems where the vertical dynamics of CO_2 and brine are important.

Acknowledgements
This work was supported in part by the National Science Foundation under grant EAR-0934722; the Department of Energy under grant DE-FE0009563; the Environmental Protection Agency under Cooperative Agreement RD-83438501; and the Carbon Mitigation Initiative at Princeton University. The authors would like to acknowledge helpful discussions with J. Nordbotten and S. Gasda.

References

Bandilla, K. W., M. A. Celia, T. R. Elliot, M. Person, K. Ellet, J. Rupp, C. Gable, and M. Dobossy (2012), Modeling carbon sequestration in the Illinois Basin using a vertically-integrated approach, *Comput. Visualization Sci.*, (15), 39–51.

Bear, J. (1972), *Dynamics of Fuids in Porous Media*, Elsevier, N. Y.

Benson, S., P. Cook, J. Anderson, and S. Bachu (2005), Underground geological storage, in *Carbon Dioxide Capture and Storage, Intergovernmental Panel on Climate Change Special Report*, edited by B. Metz et al., pp. 95–276, Cambridge Univ. Press, N. Y.

Court, B., K. W. Bandilla, M. A. Celia, A. Janzen, M. Dobossy, and J. M. Nordbotten (2012), Applicability of vertical-equilibrium and sharp-interface assumptions in CO_2 sequestration modeling, *Int. J. Green. Gas. Con.*, *10*, 134–147.

Dentz, M., and D. M. Tartakovsky (2009), Abrupt-interface solution for carbon dioxide injection into porous media, *Transp. Porous Media*, *79*(1), 15–27.

Doster, F., E. Keilegavlen, and J. M. Nordbotten (2014), A robust implicit pressure explicit mass method for multi-phase multi-component flow including capillary pressure and buoyancy, in *Computational Models for CO_2 Sequestration and Compressed Air Energy Storage*, edited by Ralfid al Khoury, and Jochen Bundschuh, Taylor and Francis Group/CRC Press, Boca Raton, Fla.

Gasda, S. E., J. M. Nordbotten, and M. A. Celia (2009), Vertical equilibrium with sub-scale analytical methods for geological CO_2 sequestration, *Comput. Geosci.*, *13*(4), 469–481.

Gasda, S. E., J. M. Nordbotten, and M. A. Celia (2011), Vertically averaged approaches for CO_2 migration with solubility trapping, *Water Resour. Res.*, *47*, W05528, doi:10.1029/2010WR009075.

Gasda, S. E., J. M. Nordbotten, and M. A. Celia (2012a), Application of simplified models to CO_2 migration and immobilization in large-scale geological systems, *Int. J. Green. Gas. Con.*, *9*, 72–84.

Gasda, S. E., H. M. Nilsen, H. K. Dahle, and W. G. Gray (2012b), Effective models for CO_2 migration in geological systems with varying topography, *Water Resour. Res.*, *48*, W10546, doi:10.1029/2012WR012264.

Hesse, M. A., H. A. Tchelepi, B. J. Cantwell, and F. M. Orr (2007), Gravity currents in horizontal porous layers: transition from early to late self-similarity, *J. Fluid Mech.*, *577*, 363–383.

Hesse, M. A., F. M. Orr, and H. A. Tchelepi (2008), Gravity currents with residual trapping, *J. Fluid Mech.*, *611*, 35–60.

Huppert, H. E., and A. W. Woods (1995), Gravity-driven flows in porous layers, *J. Fluid Mech.*, *292*, 55–69.

Juanes, R., C. W. MacMinn, and M. L. Szulczewski (2010), The footprint of the CO_2 plume during carbon dioxide storage in saline aquifers: Storage efficiency for capillary trapping at the basin scale, *Transp. Porous Media*, *82*(1), 19–30.

Lyle, S., H. E. Huppert, M. Hallworth, M. Bickle, and A. Chadwick (2005), Axisymmetric gravity currents in a porous medium, *J. Fluid Mech.*, *543*, 293–302.

Nilsen, H. M., P. A. Herrera, M. Ashraf, I. Ligaarden, M. Iding, C. Hermanrud, K.-A. Lie, J. M. Nordbotten, H. K. Dahle, and E. Keilegavlen (2011), Field-case simulation of CO2-plume migration using vertical-equilibrium models, *Energy Procedia*, *4*, 3801–3808.

Nordbotten, J. M., and M. A. Celia (2006), Similarity solutions for fluid injection into confined aquifers, *J. Fluid Mech.*, *561*, 307–327.

Nordbotten, J. M., and M. A. Celia (2012), *Geological Storage of CO_2: Modeling Approaches for Large-Scale Simulation*, John Wiley, Hoboken, N. J.

Nordbotten, J. M., M. A. Celia, and S. Bachu (2005), Injection and storage of CO_2 in deep saline aquifers: Analytical solution for CO_2 plume evolution during injection, *Transp. Porous Media*, *58*(3), 339–360.

Pacala, S., and R. Socolow (2004), Stabilization wedges: Solving the climate problem for the next 50 years with current technologies, *Science*, *305*(5686), 968–972.

Pruess, K. (2005), The TOUGH codes—A family of simulation tools for multiphase flow and transport processes in permeable media, *Vadose Zone J.*, *3*(3), 738–746.

Schlumberger (2010), ECLIPSE Technical Description, Schlumberger, Houston, Tex.

Vella, D., and H. E. Huppert (2006), Gravity currents in a porous medium at an inclined plane, *J. Fluid Mech.*, *555*, 353–362.

White, M. D., and M. Oostrom (1997), *Subsurface Transport Over Multiple Phases*, Richland, Wash.

Woods, A. W., and R. Mason (2000), The dynamics of two-layer gravity-driven flows in permeable rock, *J. Fluid Mech.*, *421*, 83–114.

Zyvoloski, G. A., B. A. Robinson, Z. V. Dash, and L. L. Trease (1997), Summary of the models and methods for the FEHM application—A finite element heat-and mass-transfer code, Los Alamos Natl. Lab., Los Alamos, N. M.